

Calculation of H₂-He Flow with Nonequilibrium Ionization and Radiation : an Interim Report

Michiko Furudate⁽¹⁾ and Keun-Shik Chang⁽²⁾

⁽¹⁾Postdoctoral Fellow, ⁽²⁾Professor

Korean Advanced Institute of Science and Technology
373-1 Guseong-dong, Yuseong-gu, Daejeon, 305-701, Korea

⁽¹⁾furufu@kaist.ac.kr; ⁽²⁾kschang-ks@kaist.ac.kr

Abstract

The nonequilibrium ionization process in hydrogen-helium mixture behind a strong shock wave is studied numerically using the detailed ionization rate model developed recently by Park which accounts for emission and absorption of Lyman lines. The study finds that, once the avalanche ionization is started, the Lyman line is self-absorbed. The intensity variation of the radiation at 5145 Å found by Leibowitz in a shock tube experiment can be numerically reproduced by assuming that ionization behind the shock wave prior to the onset of avalanche ionization is 1.3%. Because 1.3% initial ionization is highly unlikely, Leibowitz's experimental data is deemed questionable. By varying the initial electron density value in the calculation, the calculated ionization equilibration time is shown to increase approximately as inverse square-root of the initial electron density value. The true ionization equilibration time is most likely much longer than the value found by Leibowitz.

1. Introduction

In the past, on-going, and future entry flight missions to the outer planets, heating rates to the vehicle's surface tend to be large, and therefore the extent of ablation becomes also large. Therefore, accurate prediction of the heating rates becomes imperative. Computational Fluid Dynamics (CFD) can be a helpful tool in predicting the heat transfer rate if its reliability can be validated against a flight data.

The atmospheres of outer planets consist of hydrogen and helium. An entry flight into the planet Jupiter has already been accomplished in the Galileo Probe mission. Surface recession data have successfully been obtained in that mission [1]. This data is the only flight data available to validate the CFD methodology in

designing the heatshield.

The Galileo Probe data on surface recession has shown a surprisingly low surface recession in the stagnation region, and a surprisingly large recession in the downstream frustum region compared with the pre-flight predictions [2]. Very recently, Matsuyama et al [3] were able to explain the high surface recession in the downstream region by injection-induced turbulence. However, the low surface recession in the stagnation region has not yet been explained.

Park [4] has earlier speculated that the low heating in the stagnation region might be due to thermochemical nonequilibrium. The pre-flight predictions were made assuming thermochemical equilibrium. The nonequilibrium idea was first introduced by Howe [5], who derived his concept from the shock tube data of Leibowitz [6]. Leibowitz's data showed that the region immediately behind the shock wave was not ionized and did not radiate. Howe derived an empirical expression for the thickness of the non-radiating nonequilibrium region, i.e. ionization equilibration time, in a hydrogen-helium mixture.

In a companion paper to the present paper, Park [7] examined the nonequilibrium issue still further. He points out that the experiment by Leibowitz and subsequent experiment by his colleagues Livingston and Poon [8], which extended Leibowitz's data to higher flight speeds, are mostly likely erroneous because of the interaction of radiation emanating from the arc-heated driver gas. Park [7] points out that the experiment by Stalker [9] in a shock tunnel produced an equilibration time 8 times longer than that by the Leibowitz-Livingston-Poon group. Park speculates that the true equilibration time may be even longer than that determined by Stalker.

According to the experiment conducted by Bogdanoff

and Park [10], the freestream flow in front of the normal shock wave in a hydrogen-helium mixture is ionized by photo-ionization of H_2 . The temperature of the electrons so-produced is speculated to be determined indirectly by the temperature of the vibrational-rotational mode of H_2 through the electron-vibration-rotation coupling [7]. The relaxation of vibrational-rotational mode of H_2 has been studied by Furudate et al [11]. The study shows that the two modes are strongly coupled, and the temperature of the combined vib-rotational mode approaches the translational temperature relatively slowly, i.e., with a collision number of the order of hundred. The slowly rising electron temperature leads to slow initiation of the so-called avalanche ionization which sets off the rapid electron-impact ionization process that brings about the ionization equilibrium. The rate of avalanche ionization is dictated partly by the absorption of Lyman radiation [12]. Thus, the time for equilibration is dictated by the photo-ionization rate, vib-rotational relaxation rate, the coupling rate between electron temperature and vib-rotation temperature, and the rate of Lyman line absorption.

It goes without saying that further experiments should be carried out to determine the true value of the time for ionization equilibrium in hydrogen. Along with such an experiment, a CFD modeling of the phenomenon would be required. The purpose of the present paper is to carry out such a CFD modeling, and investigate how the photo-ionization, vib-rotation relaxation, electron-vib-rotational coupling, and nonequilibrium ionization proceed in a hypersonic H_2 -He flow. Because of the enormous complexity and because most of the relevant parameters are unknown, a very first simple calculation is carried out in the present work. Here, a new set of the ionization rate coefficients by Park [12] is employed. The ionization rate values used by Leibowitz in explaining his experimental data were arbitrary, and contained little physical ground. In comparison, Park's new ionization rate values are firmly based on the state-of-the-art knowledge of such a process. The electron density and electron density were first chosen arbitrarily in order to numerically reproduce Leibowitz's shock tube data [6]. The parameters controlling the initial electron density and temperature were varied to show that the ionization equilibration times can be longer than that determined by Leibowitz.

2. Methods of Calculation

2.1 Governing equations

The governing equations are the one dimensional Euler equations,

$$\frac{\partial Q}{\partial t} + \frac{\partial F}{\partial x} = W. \quad (1)$$

In the equations, the global mass, the momentum, the total energy, the species mass, and the electron energy conservation equations are included. Hence, the conservative variables Q , the convective flux vector F , and the source term W are given respectively as follows;

$$Q = \begin{pmatrix} \infty \\ \infty u \\ E \\ \infty_3 \\ E_{el} \end{pmatrix}, \quad F = \begin{pmatrix} \infty u \\ \infty u^2 + p \\ (E + p)u \\ \infty_3 u \\ E_{el} u \end{pmatrix}, \quad W = \begin{pmatrix} 0 \\ 0 \\ 0 \\ W_s \\ W_{el} \end{pmatrix} \quad (2)$$

where s stands for the chemical species, H_2 , H , H^+ , He , He^+ , e . Electron-electronic energy E_{el} in the present study is defined by

$$E_{el} = 1.5 N_e k T_e + \sum_i E_H(i) N_H(i) \quad (3)$$

where N_e is electron number density, k is Boltzmann constant, T_e is electron temperature, $E(i)$ is energy level of state i . Number density of atomic hydrogen in the state i , $N_H(i)$, is given by

$$N_H(i) = \frac{g_i \exp(-E_i / kT_e)}{\sum_i g_i \exp(-E_i / kT_e)} N_H \quad (4)$$

In the present study, first three electronic states are considered. The electron-electronic energy source term, W_{el} , can be written by

$$W_{el} = 2 N_e \sum_k \sum_{ek} \frac{m_e}{m_k} \frac{3}{2} k (T - T_e) - D W_H + \sum_i E_H(i) N_H(i) \quad (5)$$

where D is ionization energy and W_H is chemical source term for atomic hydrogen. Elastic collision frequency, ∞_{ek} , is defined by $\infty_{ek} = N_k Q_{ek} \sqrt{8kT_e / \pi m_e}$. In the present study, the elastic collision cross section, Q_{ek} , are given by the same formula as in [6].

2.2 Chemical reaction rates coefficients

The dissociation of molecular hydrogen, the ionization of atomic hydrogen, and the ionization of helium are considered. They are summarized in Table 1.

2.2.1 Rates coefficients used by Leibowitz

In [6], Leibowitz employs the idea of the two-step excitation-ionization process in his calculations; The atomic hydrogen is firstly excited by collisions (Reaction 3 and 5), and then ionizes rapidly [6]. The Electron-electronic energy E_{ei} is defined by $E_{ei} = 1.5kN_eT_e$ in [6]. The reaction rate coefficients for these reactions are summarized in Table 2. The backward reaction rates are given by the fraction of the forward reaction rates and the equilibrium constants. The equilibrium constants are summarized in Table 3. Hereafter, this approach is called the Leibowitz's method.

Table 1. Reaction

Reaction	
1	$H + e \rightleftharpoons H^+ + e + e$
2	$He + e \rightleftharpoons He^+ + e + e$
3	$H + e \rightleftharpoons H^* + e$
4	$He + e \rightleftharpoons He^* + e$
5	$H + H \rightleftharpoons H^* + H$
6	$H + He \rightleftharpoons H^* + He$
7	$H_2 + He \rightleftharpoons H + H + He$
8	$H_2 + H_2 \rightleftharpoons H + H + H_2$
9	$H_2 + H \rightleftharpoons H + H + H$
10	$H_2 + H^+ \rightleftharpoons H + H + H^+$
11	$H_2 + e \rightleftharpoons H + H + e$

Table 2. Reaction rate coefficients[6].

Reaction	Reaction Rates [m ³ /mole-s]	Ref.
1	$6.09 \times 10^{-23} \sqrt{8kT_e / \neq \infty_e} \exp(-15782/T_e)$	13
2	$3.56 \times 10^{-23} \sqrt{8kT_e / \neq \infty_e} \exp(-285248/T_e)$	14
3	$7.5 \times 10^{-22} \sqrt{8kT_e / \neq \infty_e} \exp(-11605/T_e)$	15, 16
4	$6.00 \times 10^{-23} \sqrt{8kT_e / \neq \infty_e} \exp(-23210/T_e)$	17
5	$4.0 \times 10^{-23} \sqrt{8kT / \neq \infty} \exp(-11605/T)$	
6	$4.0 \times 10^{-23} \sqrt{8kT / \neq \infty} \exp(-11605/T)$	
7	$6.93 \times 10^{-12} / T \exp(-52340/T)$	18
8	$2.5k_7$	18
9	$20.0k_7$	18
10	$20.0k_7$	
11	$20.0k_7$	

Table 3 Equilibrium constants [6].

i	Equilibrium constants, K_i [mole/m ³]
H^+	$4.05 \times 10^{-3} T^{3/2} \exp(-15872/T)$
He^+	$1.62 \times 10^{-2} T^{3/2} \exp(-285248/T)$
H	$3.7 \times 10^6 [1.0 - \exp(1.50 \times 10^8 T^{-2})] \exp(-52340/T)$

2.2.3 Park's ionization rate coefficients of atomic hydrogen accounted for radiation absorption

In order to account for the effect of the radiation absorption, the rate coefficient for the electron-impact ionization (Reaction 1) is taken from [12], and Reaction 3 is discarded. The change of electron number density due to the electron impact ionization of atomic hydrogen is expressed by

$$\frac{dN_e}{dt} = k_f N_H N_e - N_e^2 \infty_1 - N_e^2 \infty_c \infty(1), \quad (6)$$

$$\infty_1 = \infty - \infty(1) = N_e k_r + \sum_{i=2}^m \infty(i), \quad (4)$$

where k_f is the collisional ionization rate coefficient, k_r is the collisional three-body recombination rate coefficient, N_H is the atomic hydrogen number density, ∞ is the collisional-radiative recombination rate coefficient, $\infty(i)$ is the rate coefficient for radiative recombination into state i , ∞_c is Lyman continuum radiation fraction, and m is the highest bound state quantum number. Using the source code provided in [12], the parameters, k_f , k_r , ∞ and $\infty(i)$ can be obtained from the number density N_H and N_e , the electronic temperature T_e , and the Lyman line absorption factor ∞_L . The Lyman ∞ line absorption factor ∞_L is defined by

$$\infty_L = \frac{B(1, 2)}{B(1, 2)_E} = \frac{P / 1.634 \times 10^{-11} N_H(1)}{2^2 \exp[-E_H(2) / kT_e] A(2, 1)}. \quad (5)$$

where $B(i, j)$ is rate coefficient for radiative transition from lower state i to upper state j and subscript E stands for a equilibrium state. Power absorbed by the Lyman ∞ line, P , can be written by

$$P = 1.634 \times 10^{-11} A(2, 1) N(2) - \infty q_{rad}, \quad (6)$$

where ∞q_{rad} is divergence of radiative heat flux determined by solving the radiative heat transfer equation.

2.2.4. Initial electron density and temperature

Initial electron density and temperature at the onset of avalanche ionization were varied arbitrarily because they are totally unknown at this time. The relative initial electron concentration $(N_e / N_{H_2})_0$ was varied between 5×10^{-4} to 0.05, and the initial electron temperature was varied from 300 to 6000 K. The true initial electron density value is most likely lower than the lowest value considered here. However, lower initial electron density values led to numerical

instability. This problem needs to be solved in the future.

2.3 Numerical method

The convective fluxes are given by AUSM-DV upwind scheme. The dependent variables are interpolated by the MUSCL approach. An explicit Runge-Kutta method is used for time integration.

3. Test condition

A shock tube problem is numerically solved for the experimental condition of Leibowitz.³ The test gas is a mixture of 20.8% H₂-79.2% He. The driver gas is He. The measured shock velocity was 15.5 km. Using this value of shock velocity, it was impossible to numerically reproduce the measured electron density: the measured electron density values were higher. The measured electron density values were numerically reproduced assuming the shock velocity to be 16.6 km/s. The reason for such a high effective shock speed is believed to be the radiative heating of the driven gas by the radiation emitted by the driver gas [10]. The static pressure at the test section is 133 Pa. The initial translational and the electron temperature in the test section are set to 300K. The pressure ratio between the test section and the driver section is determined from the Rankine-Hugoniot relation. The computational space is 2.0 m in length and divided by 1000 cells with a constant space. The first 120 cells are considered to be the driver section.

4. Results and discussions

4.1. Leibowitz data

In order to verify the present numerical code, the reproduction of the calculated results by Leibowitz is attempted using the same reaction rates as in Leibowitz's [6]. The initial electron density is assumed to be 0%: avalanche ionization is assumed to be initiated by electrons produced mostly by Reaction 5, as in Leibowitz's work. In Fig.1, the calculated temperature profiles behind the shock wave are compared with the Leibowitz's numerical result. In the present calculation, the position of shock wave is defined by the position where translational temperature begins to increase. Differences in the temperature variation between these two calculations are initiated immediately behind the shock wave. They may be

caused by differences in the numerical methods. Note that, in Leibowitz's calculation, the equations of fluid mechanics are solved in a shock fixed coordinate system, and convections of fluids are ignored. A good agreement in the temperature is obtained in the downstream where the translational and the electron temperature are in equilibrium. Fig. 2 shows the corresponding number density profiles for atomic hydrogen and electrons. Deviation in the atomic hydrogen number density is also believed to come from the differences in the numerical methods.

In order to qualitatively examine the effect of radiation absorption on ionization of atomic hydrogen, calculations with Park's ionization rate at three fixed values of the Lyman line absorption factor α_L are implemented. The values of $\alpha_L = 0, 1$ and 100 are chosen, representing an optically thin case, a

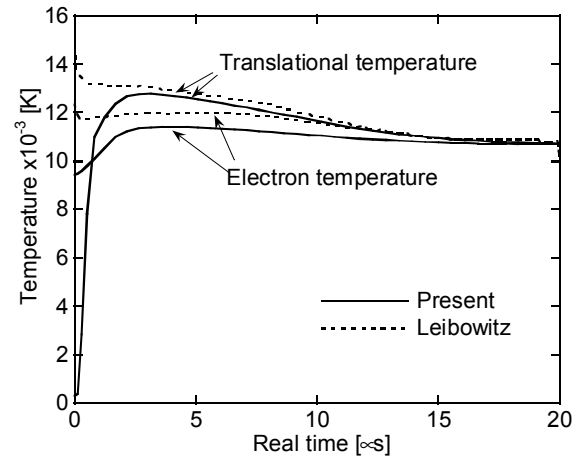


Fig. 1 Temperatures profile obtained in the present calculation.

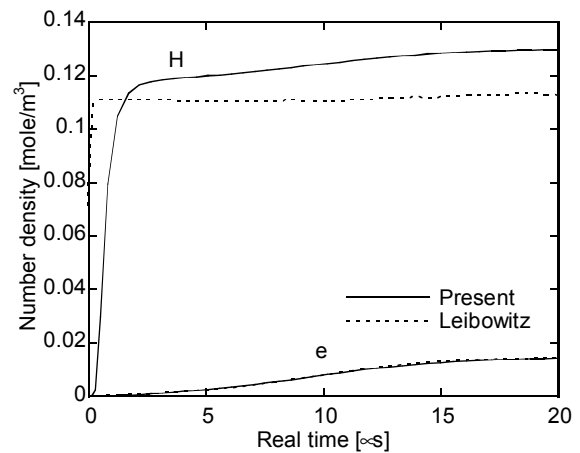


Fig. 2 Number density profile obtained in the present calculation.

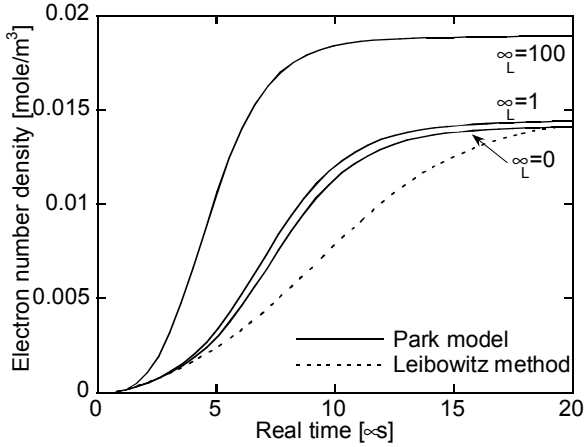


Fig. 3 Effect of Lyman radiation on electron number density profile.

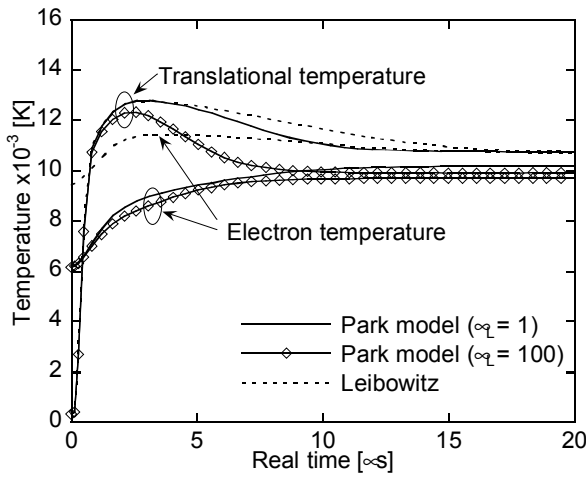


Fig. 4 Effect of Lyman radiation on temperatures profile.

self-absorbed case, and a strongly irradiated case, respectively. For all the cases here, the Lyman continuum radiation fraction α_c is set to 1. Fig. 3 shows the number density profiles obtained in the present calculations. The electron number density stays low in the first few microseconds behind shock wave, where the collisional ionization (Reaction 5) is dominant. Then, an avalanche ionization zone appears where the electron-impact ionization is dominant. In the cases for higher α_L , incubation time to initiate the avalanche ionization is shorter, and the rate of electron production during the avalanche ionization is faster. The electron number density at the quasi-steady state (QSS), which appears after the avalanche ionization ends, is also affected by α_L . In the strongly irradiated case of $\alpha_L = 100$, the electron number density at the

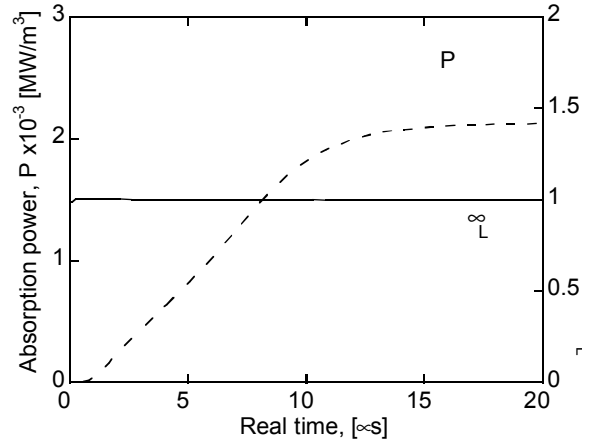


Fig. 5 Radiative power absorbed by the Lyman ∞ line and Lyman line absorption factor behind shock wave.

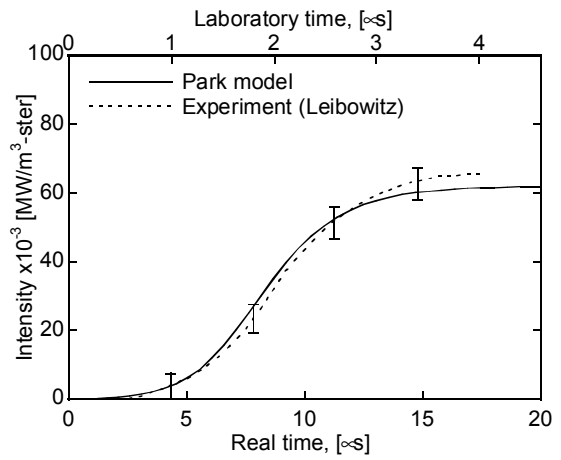


Fig. 6 Calculated radiative intensity and the experimental data by Leibowitz ($\infty = 5145 \text{ \AA}$).

QSS is 30 % larger than the case of $\alpha_L = 0$. The temperature profiles are also drastically changed according to the value of α_L , as shown in Fig 4. The high degree of electron impact ionization with the large value of α_L lowers the electron temperature in the ionization zone. Accordingly, equilibrations between the translational and the electron temperature proceed faster.

The variation of the value of α_c gives a minor effect on the flowfield. Although the figure is not shown here, the electron number density profiles with $\alpha_c = 0.5$ are almost identical to the results with $\alpha_c = 1$ when the value of α_L is fixed.

A calculation using local values of α_L , which is determined by solving the heat transfer equation, is

performed next. The heat transfer equation is solved using a multi-band model. Absorption coefficients for the Lyman ∞ line are evaluated at 23 wavelength points in the range from 1200 to 1230 Å. The calculated radiation power of absorption by the Lyman ∞ line and the Lyman line absorption factor α_L are shown in Fig. 5. The radiation power of absorption varies from 0 in the non-ionization zone behind the shock wave to about 2000 MW/m³ in the QSS zone in the down stream. The Lyman ∞ line absorption factor α_2 keeps constant at the value nearly equal to 1 after slight increase immediately behind the shock wave; the emission from Lyman ∞ line is totally absorbed. Therefore, the electron number density and the temperatures profiles are almost identical to those in the case of $\alpha_L=1$ in Fig 3 and 4. The calculated radiative intensity profile for the wavelength of 5145 Å is compared with the experimental data in Fig. 6. The same approach as in [3] is employed to calculate the intensity. The obtained intensity profile agrees well with the experimental data measured by Leibowitz.

4.2. Effect of initial electron density and temperature

In this subsection, effects of initial electron number density and electron temperature are examined by a parametric study. For the calculations in this study, Reaction 5 and 6 in Table 1 is discarded, and the initial number density at the point of initiation of avalanche ionization is given at a certain value. From the observation in the previous subsection, $\alpha_2=1$ and $\alpha_3=1$ are employed for all the cases in this subsection.

First, the ratio of the initial electron number density to the initial molecular hydrogen is varied, while the initial electron temperature is remained to be 300K. As shown in Fig. 7, the intensity profile for 5145 Å is changed according to variation of $(N_e/N_{H_2})_0$. Leibowitz's experimental data can be reproduced with $(N_e/N_{H_2})_0 = 0.013$. The initiation and the degree of avalanche ionization of atomic hydrogen are greatly affected by the initial electron number density, as shown in the electron number density profile in Fig. 8. Larger non-ionization region is obtained with lower initial electron number density.

Next, the initial electron temperature, T_{e0} , is varied from 300 to 6000 K, while the initial $(N_e/N_{H_2})_0$ is

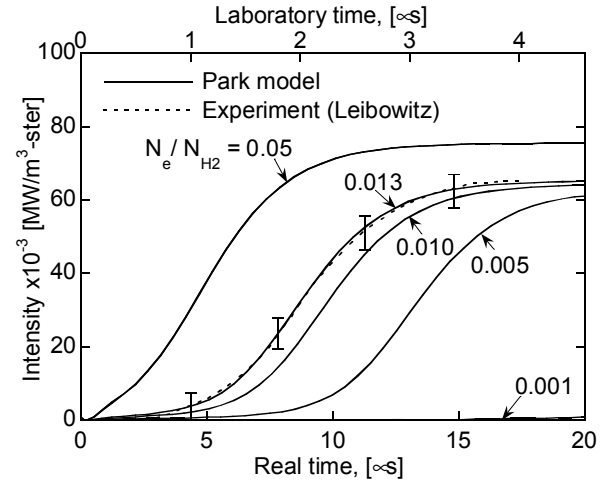


Fig. 7 Effect of initial electron number density on intensity profile.

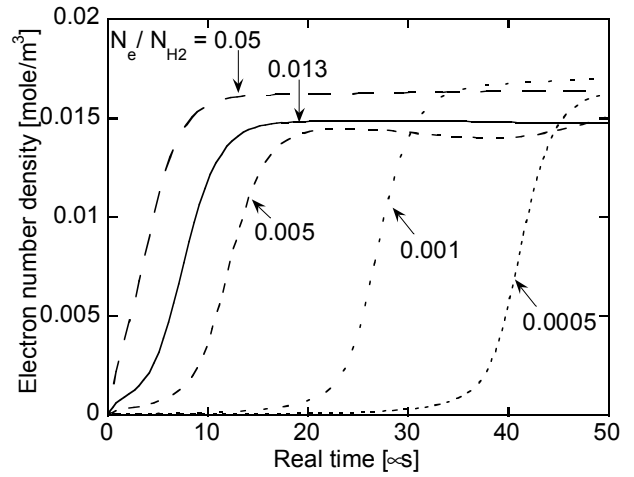


Fig. 8 Effect of initial electron number density on electron number density profile. ($T_{e0} = 300$ K).

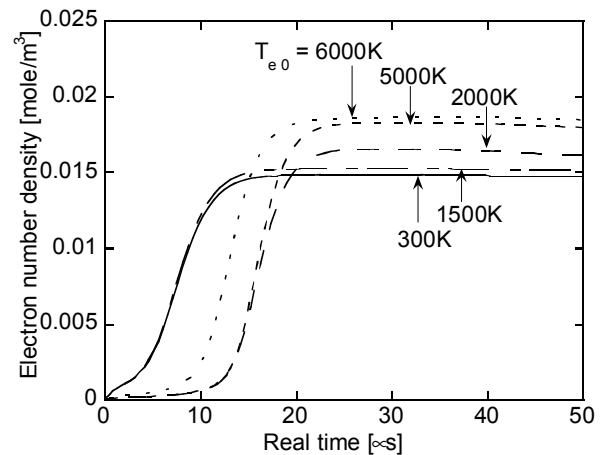


Fig. 9 Effect of initial electron temperature on electron number density profile ($(N_e/N_{H_2})_0 = 0.013$).

fixed at the value of 0.013. The initial electron temperature at the point of initiation of avalanche ionization is at presently totally unknown. The electron number density profiles obtained for the various value of T_{e0} are shown in Fig. 9. For $2000 < T_{e0} < 5000\text{K}$, times to initiate the avalanche ionization are almost identical, although higher temperature gives more production of electrons. The time to reach QSS with $T_{e0} = 2000$ is about two times large than that of 300 K. For the T_{e0} higher than 2000K, the time to QSS becomes shorter as the temperature increases. It is interesting to see that the effect of high initial electron temperature is not monotonic: the longest delay of ionization occurs at electron temperature of 2000 K.

Fig. 10 summarizes the effect of the initial electron number density on the e-folding ionization equilibrium time. For all the initial electron temperature cases, the equilibration time increases according to the $(N_e / N_{H_2})_0$ decrease. When the initial electron number density is lower, the effect of initial electron temperature is minor. The equilibration time for $(N_e / N_{H_2})_0 = 0.0005$ is about 5 times longer than that for $(N_e / N_{H_2})_0 = 0.013$ at $T_{e0} = 300\text{K}$. For $T_{e0} = 300\text{K}$, the ionization equilibration time varies approximately as inverse square-root of the initial electron density.

5. Discussion

In this study, only the avalanche ionization process is modeled. We find first that, once avalanche ionization process is started, the absorption of Lyman lines is of little consequence, because it is nearly totally self-absorbed. However, we do not yet know how Lyman radiation will affect the region prior to the avalanche ionization.

Another important finding here is that the time to reach ionization equilibrium is affected strongly by the initial electron density and temperature at the point of avalanche ionization. In the range of the initial electron density values considered in the present work, a factor of 5 variation is seen. As mentioned in 2.2.4, the lowest value of initial electron density was set in the present work by the numerical instability. The true initial electron density is most likely lower than the value considered in the present work. In the region ahead of avalanche ionization, photo-ionization process is the only mechanism to produce the initial electrons. Because electron temperature will be low in

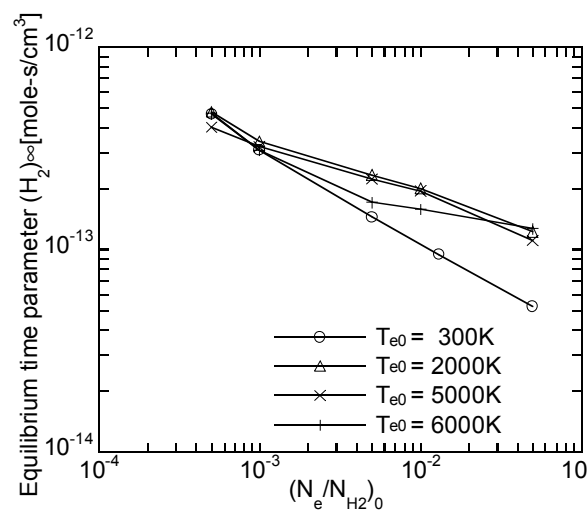


Fig. 10 Effect of initial electron number density and initial electron temperature on the ionization equilibrium time.

the region, the free electrons produced by photo-ionization will be rapidly recombining. The present work finds that Leibowitz's shock tube data can be numerically reproduced with an initial $(N_e / N_{H_2})_0$ value of 0.013, i.e. 1.3% ionization. This value of 1.3% is much higher than the value found experimentally by Bogdanoff and Park [10], and should be considered impossible. The only explanation is the photo-ionization by the strong radiation transmitted from the arc-heated driver gas [10].

According to Fig. 10, equilibration time increases roughly as an inverse square-root of the initial electron density, as mentioned. If the true value of $(N_e / N_{H_2})_0$ is 10^{-6} , the equilibration time will be two orders of magnitude longer than Leibowitz's value. The equilibration time value of Stalker [9], which is 8 times larger than the value by Leibowitz, is well within the explainable range. This means that, at this time, we do not know how to predict the thickness of the nonequilibrium, un-ionized, non-radiating region behind the shock wave in outer planet entry flights. This points to the need to know more about the processes occurring in the region prior to the initiation of avalanche ionization.

6. Conclusions

Using the detailed ionization rate model developed recently by Park, it is found that the absorption of Lyman alpha has a great influence on the initiation and

the rate of avalanche ionization behind a shock wave. For a strong absorption, avalanche ionization initiates earlier and faster. Once the avalanche ionization is started, the Lyman line absorption behind shock wave is almost constant at the value of 1, which represents the emission from Lyman line is self-absorbed by the atomic hydrogen gas. The calculated intensity profile for 5145 Å agrees well with the experimental data by Leibowitz, when the starting degree of ionization is assumed to be 1.3%, which is unrealistically high. The ionization equilibration time is roughly inversely proportional to the square-root of the initial electron density, which are presently unknown. The true ionization equilibration time could be up to two orders of magnitude longer than that determined by Leibowitz.

7. Acknowledgments

The authors would like to express their appreciation to Prof. Chul Park, Korean Advanced Institute of Science and Technology, Korea, for helpful comments and suggestions.

8. References

1. Milos, F. S., "Galileo Probe Heat Shield Ablation Experiment," *Journal of Spacecraft and Rockets*, Vol. 31, No. 6, November-December 1997, pp. 705-713.
2. Moss, J. N., and Simmonds, A. L., "Galileo Probe Forebody Flowfield Predictions," Entry Vehicle Heating and Thermal Protection Systems: Space Shuttle, Solar Starprobe, Jupiter Galileo Probe, *Progress in Astronautics and Aeronautics*, Vol. 85, edited by P. E. Bauer and H. E. Collicott, AIAA New York, 1983, pp. 419-445.
3. Matsuyama, S., Ohnishi, N., Sasoh, A., and Sawada, K., "Numerical Simulation of Galileo Probe Entry Flowfield with Radiation and Ablation," *AIAA Paper 2002-2994*; to be published in *Journal of Thermophysics and Heat Transfer*.
4. Park, C., "Heatshielding Problems of Planetary Entry, A Review," *AIAA Paper 99-3415*, June 1999.
5. Howe, J. T., "Hydrogen Ionization in the Shock Layer for Entry into the Outer Planets," *AIAA Journal*, Vol. 12, No. 6, June 1974, pp. 875-876.
6. Leibowitz, L. P., "Measurements of the Structure of an Ionizing Shock Wave in a Hydrogen-Helium Mixture," *The Physics of Fluids*, Vol. 16, No. 1, January 1973, pp. 59-68.
7. Park, C., "On Nonequilibrium Radiation in Hydrogen Shock Layers," paper presented at the 2nd Probe Workshop, NASA Ames Research Center, August 2004.
8. Livingston, F. R., and Poon, P. T. Y., "Relaxation Distance and Equilibrium Electron Density Measurements in Hydrogen-Helium Plasmas," *AIAA Journal*, Vol. 14, No. 9, September 1976, pp. 1335-1337.
9. Stalker, R. J., "Shock Tunnel Measurement of Ionization Rates in Hydrogen," *AIAA Journal*, Vol. 18, No. 4, April 1980, pp. 478-480.
10. Bogdanoff, D. A., and Park, C., "Radiative Interaction Between Driver and Driven Gases in an Arc-Driven Shock Tube," *Shock Wave*, Vol. 12, No. 3, November 2002, pp. 205-214.
11. Furudate, M., Fujita, K., and Abe, T., "Coupled Rotational-Vibrational Relaxation of Molecular Hydrogen at High Temperatures," *AIAA Paper 2003-3780*.
12. Park, C., "Effect of Lyman Radiation on Nonequilibrium Ionization of Atomic Hydrogen," *AIAA Paper 2004-2277*, June 2004.
13. Wade L. Fite and R. T. Brackmann, "Collisions of Electrons with Hydrogen Atoms. I. Ionization," *Physical Review*, vol. 112, 1958, pp. 1141-1151.
14. H. Massey and E. Burhop, *Electronic and Ionic Impact Phenomena*, Oxford, 1952, p.38.
15. J. W. McGowan, J. F. Williams*, and E. K. Curley, "e-H Resonances in the 2p Excitation Channel," *Physical Review*, vol. 180, 1969, pp. 132-138.
16. W. E. Kauppila, W. R. Ott, and W. L. Fite, "Excitation of Atomic Hydrogen to the Metastable 2²S_{1/2} State by Electron Impact", *Physical Review A*, vol.1, 1970, pp. 1099-1108.
17. H. Holt and R. Krotkov, "Excitation of n=2 States in Helium by Electron Bombardment," *Physical Review*, vol. 144, 1966, pp. 82-93.
18. T. Jacobs, R. Giedt, and N. J. Cohen, "Kinetics of Hydrogen Halides in Shock Waves. II. A New Measurement of the Hydrogen Dissociation Rate", *The Journal of Chemical Physics*, vol.47, 1967, pp. 54-57.